Atmos. Meas. Tech., 10, 445–458, 2017
www.atmos-meas-tech.net/10/445/2017/
doi:10.5194/amt-10-445-2017
© Author(s) 2017. CC Attribution 3.0 License.

Atmospheric Measurement Techniques
Open Access
EGU

New-generation NASA Aura Ozone Monitoring Instrument (OMI) volcanic SO_2 dataset: algorithm description, initial results, and continuation with the Suomi-NPP Ozone Mapping and Profiler Suite (OMPS)

Can Li[1,2], Nickolay A. Krotkov[2], Simon Carn[3], Yan Zhang[1,2], Robert J. D. Spurr[4], and Joanna Joiner[2]

[1]Earth System Science Interdisciplinary Center, University of Maryland, College Park, MD 20742, USA
[2]NASA Goddard Space Flight Center, Greenbelt, MD 20771, USA
[3]Department of Geological and Mining Engineering and Sciences, Michigan Technological University, Houghton, MI 49931, USA
[4]RT Solutions, Inc., Cambridge, MA 02138, USA

Correspondence to: Can Li (can.li@nasa.gov)

Received: 1 July 2016 – Published in Atmos. Meas. Tech. Discuss.: 13 September 2016
Revised: 1 January 2017 – Accepted: 15 January 2017 – Published: 6 February 2017

Abstract. Since the fall of 2004, the Ozone Monitoring Instrument (OMI) has been providing global monitoring of volcanic SO_2 emissions, helping to understand their climate impacts and to mitigate aviation hazards. Here we introduce a new-generation OMI volcanic SO_2 dataset based on a principal component analysis (PCA) retrieval technique. To reduce retrieval noise and artifacts as seen in the current operational linear fit (LF) algorithm, the new algorithm, OMSO2VOLCANO, uses characteristic features extracted directly from OMI radiances in the spectral fitting, thereby helping to minimize interferences from various geophysical processes (e.g., O_3 absorption) and measurement details (e.g., wavelength shift). To solve the problem of low bias for large SO_2 total columns in the LF product, the OMSO2VOLCANO algorithm employs a table lookup approach to estimate SO_2 Jacobians (i.e., the instrument sensitivity to a perturbation in the SO_2 column amount) and iteratively adjusts the spectral fitting window to exclude shorter wavelengths where the SO_2 absorption signals are saturated. To first order, the effects of clouds and aerosols are accounted for using a simple Lambertian equivalent reflectivity approach. As with the LF algorithm, OMSO2VOLCANO provides total column retrievals based on a set of predefined SO_2 profiles from the lower troposphere to the lower stratosphere, including a new profile peaked at 13 km for plumes in the upper troposphere. Examples given in this study indicate that the new dataset shows significant improvement over the LF product, with at least 50 % reduction in retrieval noise over the remote Pacific. For large eruptions such as Kasatochi in 2008 ($\sim$ 1700 kt total SO_2) and Sierra Negra in 2005 (> 1100 DU maximum SO_2), OMSO2VOLCANO generally agrees well with other algorithms that also utilize the full spectral content of satellite measurements, while the LF algorithm tends to underestimate SO_2. We also demonstrate that, despite the coarser spatial and spectral resolution of the Suomi National Polar-orbiting Partnership (Suomi-NPP) Ozone Mapping and Profiler Suite (OMPS) instrument, application of the new PCA algorithm to OMPS data produces highly consistent retrievals between OMI and OMPS. The new PCA algorithm is therefore capable of continuing the volcanic SO_2 data record well into the future using current and future hyperspectral UV satellite instruments.

1 Introduction

Volcanic emissions, while collectively a smaller source of sulfur dioxide (SO_2) than anthropogenic emissions (e.g., Bluth et al., 1993), are a dominant and highly variable natural forcing to the Earth's climate system. Explosive eruptions such as El Chichón in 1982 (Krueger, 1983) and Mt. Pinatubo

in 1991 (McCormick et al., 1995, and references therein) directly inject large amounts of SO_2 and other species into the stratosphere, producing secondary sulfate aerosols that can remain at high altitudes for years. Such large eruptions are rare, but they have been found to cause significant perturbations to global surface temperature and atmospheric circulation patterns (e.g., Robock and Mao, 1995; Robock et al., 2007; Stenchikov et al., 2002). Recent studies (Ridley et al., 2014; Solomon et al., 2011; Vernier et al., 2011) suggest that more frequent, moderate eruptions may also be a far more important source of stratospheric aerosols than previously thought and may have contributed to the slower recent rate of global warming (Santer et al., 2014). SO_2 emitted by passive volcanic degassing is normally too short-lived to reach the stratosphere, but its regional climate impact can be significant through the interaction between secondary sulfate aerosols and clouds (Schmidt et al., 2012; Yuan et al., 2011). In addition to their climate effects, volcanic plumes also pose severe threats to health and human lives and aviation safety (e.g., Carn et al., 2009; Stohl et al., 2011). To better understand volcanic climate forcing, it is important to acquire accurate estimates of emissions from various types of volcanic activity. Mitigating volcanic hazards, in contrast, requires global monitoring of volcanic plumes on a timely basis.

Since the first demonstration by Krueger (1983), satellite retrievals of volcanic SO_2 using ultraviolet (UV) instruments have become a critical tool in studies of volcanism as well as in management of aviation safety. The satellite volcanic SO_2 data record dates back to the 1970s (e.g., Carn et al., 2016). However, earlier measurements (pre-1990s) were generally limited to larger eruptions (e.g., Krueger et al., 1995; McPeters, 1993) due to the small number of discrete wavelengths and relatively large footprint size characteristic of heritage instruments such as the Total Ozone Mapping Spectrometer (TOMS). Since the 1990s, hyperspectral UV instruments have made measurements at hundreds of wavelengths, allowing SO_2 absorption features to be more clearly separated from interfering processes. This has been demonstrated with the Global Ozone Monitoring Experiment (GOME; Burrows et al., 1999; Eisinger and Burrows, 1998), GOME-2 (Nowlan et al., 2011; Rix et al., 2009), and the SCanning Imaging Absorption spectroMeter for Atmospheric CHartographY (SCIAMACHY; Lee et al., 2008).

Among hyperspectral instruments that are currently operating in orbit, the Dutch–Finnish Ozone Monitoring Instrument (OMI; Levelt et al., 2006), launched on board NASA's Aura spacecraft in 2004, offers the best ground resolution ($13 \times 24\,km^2$ at nadir), along with a wide spectral range (270–500 nm) and contiguous daily global coverage – features that make it an effective instrument for global SO_2 monitoring. In contrast to TOMS, OMI permits the detection of weak SO_2 emissions such as those from coal-fired power plants or quiescent degassing volcanoes (e.g., Carn et al., 2008; Hsu et al., 2012; Li et al., 2010a, b; Lu et al., 2010), even with the at-launch algorithms (Krotkov et al., 2006, 2008; Yang et al., 2007) that utilize only a small fraction of the available wavelengths. The linear fit (LF) algorithm (Yang et al., 2007) is presently the operational algorithm for NASA's standard OMI volcanic SO_2 product. It uses 10 OMI wavelengths between 310.8 and 360.2 nm and produces estimates of the total SO_2 vertical column density (VCD) assuming three different prescribed SO_2 profiles with center of mass altitudes (CMAs) at 3 km (lower troposphere, TRL), 8 km (middle troposphere, TRM), and 18 km (lower stratosphere, STL). The presumed CMAs were selected to represent SO_2 from passively degassing volcanoes, moderate eruptions, and large explosive eruptions, respectively. In addition to the OMI standard product, the LF algorithm has also been implemented to produce SO_2 retrievals quickly from direct readout data, as well as near-real-time SO_2 data from OMI and the Ozone Mapping and Profiler Suite (OMPS) nadir mapper aboard the NASA/NOAA Suomi National Polar-orbiting Partnership (Suomi-NPP) spacecraft. The LF algorithm has been widely used in studies of volcanic SO_2 and aviation safety applications, but it has a number of limitations. For example, it is known to significantly underestimate SO_2 VCDs in relatively large eruptions due to signal saturation at shorter wavelengths (e.g., Krotkov et al., 2010; Yang et al., 2009a). The algorithm also has large biases over clean background areas, making it difficult to track volcanic plumes from relatively small eruptions.

Several studies have demonstrated that OMI SO_2 retrievals can be improved by exploiting the full spectral content of the hyperspectral OMI measurements. Theys et al. (2015) produced an OMI SO_2 product with reduced noise and bias using a DOAS (Differential Optical Absorption Spectroscopy) scheme. For large volcanic signals, they used longer wavelengths (up to 360–390 nm) where SO_2 is only weakly absorbing to avoid signal saturation. The iterative spectral fitting (ISF, and its variant, direct spectral fitting or DSF) algorithm developed by Yang et al. (2009a) also utilized OMI spectral measurements at longer wavelengths and produced much greater SO_2 VCDs for SO_2-rich eruptions such as Sierra Negra in 2005 (Yang et al., 2009a) and Kasatochi in 2008 (Krotkov et al., 2010) than the corresponding VCDs derived from the LF algorithm. However, the ISF/DSF algorithm relies on computationally intensive online radiative transfer calculations and instrument-specific soft calibration, hindering its operational implementation.

Recently, we introduced a retrieval technique based on principal component analysis (PCA) of satellite-measured radiances (Li et al., 2013, 2015). Unlike DOAS or ISF/DSF, the PCA technique is a data-driven approach and uses a set of principal components (PCs) extracted directly from satellite radiance data in the spectral fitting. It benefits from the fact that the PCs that account for the most spectral variance have characteristics associated with various geophysical processes (e.g., O_3 absorption, rotational Raman scattering or RRS) or measurement details (e.g., wavelength shift, varia-

tion in dark current). This allows these various interferences in SO_2 retrievals to be minimized without extensive forward calculation or explicit instrument characterization, leading to an efficient implementation with relatively small biases and noise in the retrieved SO_2 VCDs.

Our PCA algorithm has been implemented for operational production of the new-generation NASA standard OMI planetary boundary layer (PBL) SO_2 dataset (used for air quality studies). As compared with the previous OMI PBL SO_2 dataset (Kroktov et al., 2006), the new product improves the detection limit for point anthropogenic sources by a factor of two (Fioletov et al., 2015, 2016), enabling the detection of a large number of sources missing in current emission inventories (McLinden et al., 2016). The reduced retrieval bias also makes it easier to detect regional trends of SO_2 (e.g., Krotkov et al., 2016). He et al. (2016) demonstrated that, without extensive bias correction, it was possible to derive a clear regional SO_2 trend over the eastern US from the new PCA product but not from the previous product. In this paper, we extend the PCA algorithm to volcanic retrievals and introduce the new-generation NASA OMI volcanic SO_2 product. We describe the algorithm in Sect. 2 and present results for selected scenarios in Sect. 3, including background regions and several volcanic eruptions; the focus is on comparisons with retrievals from the current operational LF algorithm. Another advantage of the PCA approach is its ability to generate consistent retrievals between different instruments, and in Sect. 4 we discuss the prospect of continuing the long-term OMI data record with Suomi-NPP OMPS.

2 Algorithm description

Our new OMI volcanic SO_2 algorithm (hereafter referred to as OMSO2VOLCANO) comprises two main components: the first step (enclosed by the dashed blue box in the algorithm flowchart; Fig. 1) is designed to identify pixels having strong SO_2 signals and provide initial estimates of SO_2 VCD (Ω_{SO_2}). The second step produces more accurate estimates of volcanic SO_2 VCD through iterative spectral fitting.

2.1 Step 1: PCA and initial fit

The first step of the OMSO2VOLCANO algorithm is essentially identical to the operational OMI PBL SO_2 algorithm that has been previously described in detail elsewhere (Li et al., 2013) and is only briefly reviewed here. In short, for each OMI orbit, we process the 60 rows (cross-track positions) one at a time, employing a PCA technique to extract PCs (v_i) for the spectral range 310.5–340 nm from the sun-normalized radiance spectra of $\sim$1000 pixels along the flight direction (after excluding pixels with high slant column ozone). The PCs are ranked in descending order according to the spectral variance they each explain. If derived from SO_2-free regions, the first several PCs that account for the most of the variance are representative of geophysical processes unrelated to SO_2 such as ozone absorption and RRS, as well as measurement details such as wavelength shift. We then obtain initial estimates of SO_2 VCD ($\Omega_{SO_{2\_ini}}$) and the coefficients of the PCs (ω) by fitting the first n_v (non-SO_2) PCs and the SO_2 Jacobians ($\partial N/\partial\Omega_{SO_2}$) to the measured radiance spectrum (in this case the quantity N, which is the logarithm of the sun-normalized radiances, I):

$$N\left(\omega,\Omega_{SO_2}\right)=\sum_{i=1}^{n_v}\omega_i v_i+\Omega_{SO_2}\frac{\partial N}{\partial\Omega_{SO_2}}. \quad (1)$$

The SO_2 Jacobians represent the sensitivity of sun-normalized backscattered radiances (I or its logarithm, N) at the top of the atmosphere (TOA) to a unit perturbation in Ω_{SO_2} and were precalculated with the vector radiative transfer code VLIDORT (Spurr, 2008). As with the PBL SO_2 algorithm (Li et al., 2013), in this part of the algorithm we use a fixed SO_2 Jacobian spectrum in Eq. (1), calculated assuming that SO_2 is predominantly in the lowest 1000 m of the atmosphere and that the observation is made under cloud-free conditions with fixed surface albedo (0.05), surface pressure (1013.25 hPa), solar zenith angle (30°), viewing zenith angle (0°), and preset O_3 and temperature profiles (with O_3 VCD = 325 DU).

In most cases, we use $n_v = 20$ PCs in the fitting. However, in the presence of strong SO_2 signals (e.g., a volcanic plume), the inclusion of that many PCs in Eq. (1) can introduce collinearity, as some of the leading PCs may contain an SO_2 absorption signature. To avoid this, we examine the PCs 4–20 and only use $n_v = i - 1$ PCs if the ith PC is found to be significantly correlated with SO_2 cross sections at the 95 % confidence level. Note that we always include the first three PCs in fitting, as they are clearly associated with geophysical processes such as O_3 absorption (Li et al., 2013). An example of the correlation coefficients between SO_2 and PCs is given in Fig. S1 in the Supplement to further demonstrate this technique. We then exclude pixels with large $\Omega_{SO_{2\_ini}}$ (outside of $\pm$1.5 standard deviations for the row) and repeat the PCA and spectral fitting to get updated PCs and the SO_2 VCD. The output PCs and VCD are used as input to the second step of the OMSO2VOLCANO algorithm (see Fig. 1).

2.2 Step 2: Volcanic SO_2 Jacobians lookup table (LUT)

A main function of the second step of the OMSO2VOLCANO algorithm is to determine SO_2 Jacobians under various actual observation conditions. In our spectral range of interest ($\sim$310 to 340 nm), both I (i.e., sun-normalized backscattered radiances at TOA) and the SO_2 Jacobians depend on a number of factors including satellite geometry (solar zenith angle, SZA or θ_0, viewing zenith angle, VZA or θ, and relative azimuth angle, RAZ or ϕ), surface reflectivity and pressure, cloud fraction and height, aerosols, and the amount and vertical distribution of absorbing gases (O_3 and SO_2). However, for an operational

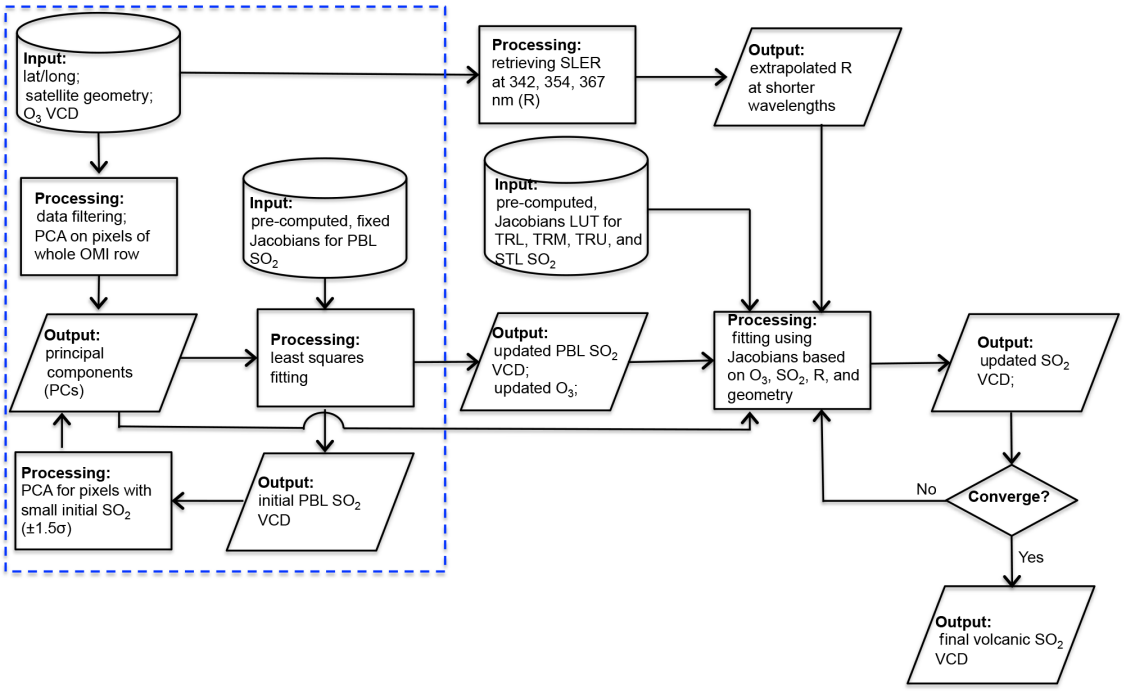

Figure 1. A flow chart of the new OMI volcanic SO_2 PCA retrieval algorithm (OMSO2VOLCANO). The first part of the algorithm, enclosed in the dashed blue box, is essentially identical to the operational OMI planetary boundary layer (PBL) SO_2 algorithm (Li et al., 2013) and provides input to the second part of algorithm that performs iterative spectral fitting to retrieve volcanic SO_2 VCD.

global retrieval algorithm, it would be too computationally expensive to perform online radiative transfer calculations at many wavelengths to explicitly account for all of these factors. Moreover, some of these factors, such as the height of the volcanic SO_2 plume or the composition and size distribution of aerosols, are usually not well known or well defined at the time of retrieval. To simplify the problem and save computational expense, we have constructed a number of pre-computed LUTs for volcanic SO_2 Jacobians, following an approach similar to that used in TOMS and OMI total column O_3 retrievals (Bhartia and Wellemeyer, 2002). We assume that, to first order, the combined effects of clouds/aerosols/surface reflectivity on SO_2 Jacobians are accounted for with a simple Lambertian equivalent reflectivity (SLER or R) derived at the surface (Ahmad et al., 2004). We also neglect the effects of inelastic RRS on SO_2 Jacobians (RRS contribution to radiances is accounted for with PCs in Eq. 1). On the basis of these assumptions, the backscattered radiances at TOA (I) for Rayleigh multiple scattering can be calculated with the following equation:

$$I = I_0(\theta_0,\theta) + I_1(\theta_0,\theta)\cos\phi + I_2(\theta_0,\theta)\cos 2\phi + \frac{RI_r(\theta_0,\theta)}{(1-RS_b)}. \quad (2)$$

The first three terms (I_0, I_1, and I_2) on the right-hand side of Eq. (2) are Fourier expansion coefficients in azimuthal angle that in the case of Rayleigh scattering have only two terms (Dave, 1964). Together, they represent the atmospheric contribution to the radiances. The last term represents the surface contribution, where RI_r represents the TOA radiance that is reflected once from the surface and transmitted through the atmosphere, and $(1-RS_b)$ accounts for the effects of multiple reflections between the surface and the atmosphere, with S_b being the fraction of surface-reflected radiation that is scattered back to the surface by the atmosphere. Note that these terms also depend on absorbing gases such as O_3 and SO_2, which are omitted from Eq. (2) for brevity. Equation (2) has been used widely in satellite backscattered UV (BUV) retrievals of ozone and other minor gaseous components (e.g., Bhartia and Wellemeyer, 2002), as it allows for the use of smaller LUTs by excluding the azimuth dimension. Taking the partial derivative with respect to the SO_2 VCD (Ω_{SO_2}), we obtain the following equation for the calculation of SO_2 Jacobians:

$$\frac{\partial I}{\partial \Omega_{SO_2}} = \frac{\partial I_0(\theta_0,\theta)}{\partial \Omega_{SO_2}} + \frac{\partial I_1(\theta_0,\theta)}{\partial \Omega_{SO_2}}\cos\phi + \frac{\partial I_2(\theta_0,\theta)}{\partial \Omega_{SO_2}}\cos 2\phi + \frac{R}{(1-RS_b)}\frac{\partial I_r(\theta_0,\theta)}{\partial \Omega_{SO_2}} + \frac{R^2 I_r(\theta_0,\theta)}{(1-RS_b)^2}\frac{\partial S_b}{\partial \Omega_{SO_2}}. \quad (3)$$

To account for O_3 vertical distributions, we generated a set of SO_2 Jacobian LUTs, one for each of the 21 standard O_3 climatology profiles used in OMI total O_3 retrievals (each

profile represents an O_3 node), employing VLIDORT (Spurr, 2008) to compute the components in Eq. (3) (I_0, I_1, I_2, I_r, S_b, and their derivatives with respect to Ω_{SO_2}) for 8 SZAs (0–81°), 8 VZAs (0–80°), and 15 SO_2 nodes (0–1000 DU) for the spectral range 311–342 nm at 0.05 nm resolution (see Table 1 for a list of the nodes). This was done for four prescribed Gaussian vertical SO_2 profiles with a full width at half maximum (FWHM) of ∼ 2.3 km and different CMAs. Three of these profiles have the same plume CMAs as those used in the LF algorithm (3 km or TRL, 8 km or TRM, and 18 km or STL). Retrievals produced using these profiles are distributed as part of the new operational OMI SO_2 dataset (OMSO2 V1.3.0). The fourth SO_2 profile, centered at 13 km altitude, was introduced for the generation of a new TRU (upper troposphere) SO_2 research product. Several eruptions during the OMI era, including Kasatochi in 2008, injected SO_2 to altitudes between 8 and 18 km, and the TRU profile should allow for more accurate retrievals for those eruptions.

2.3 Step 2: Ancillary retrieval parameters, data processing, and fitting windows

For a given pixel with SZA = θ_0, VZA = θ, and RAZ = ϕ, a number of ancillary retrieval parameters are generated at intermediate steps in the OMSO2VOLCANO algorithm, before the volcanic SO_2 Jacobians for the pixel can be determined. Two of these parameters, namely the initial estimate of SO_2 VCD ($\Omega_{SO_2\_ini}$) and an estimate of O_3 VCD (Ω_{O_3}), come from the first stage of the OMSO2VOLCANO algorithm (blue box in Fig. 1). Ω_{O_3} is from the operational OMI total column O_3 product (OMTO3) for most pixels but, for pixels having large SO_2 signals ($\Omega_{SO_2\_ini} > 5$ DU), it is interpolated from neighboring pixels with small $\Omega_{SO_2\_ini}$ in order to avoid overestimation of Ω_{O_3} due to SO_2 contamination. For the SLER (R), we first derive R at 342.5, 354.1, and 367.04 nm by matching the measured and calculated radiances in Eq. (2). Since contributions from gaseous absorption and RRS processes are minimal at these wavelengths, we use a smaller LUT and assume a fixed O_3 profile ($O_3 = 325$ DU). We then fit a second-degree polynomial function to the three wavelengths to extrapolate R to shorter wavelengths. The interpolation implicitly accounts for the combined effects of aerosols, clouds, and the surface on the spectral dependence of TOA radiances. An example of the derived R is given in Fig. S2.

For each presumed SO_2 profile, the algorithm then selects two pre-computed LUTs based on the O_3 VCD and the latitude of the pixel, with the two O_3 nodes bracketing the input Ω_{O_3} for the pixel ($\Omega_{node1} < \Omega_{O_3} < \Omega_{node2}$). For the lookup table with O_3 VCD = Ω_{node1}, a total of eight SO_2 Jacobian spectra are calculated using ϕ and the derived R as input to Eq. (3) for two SO_2, two SZA, and two VZA nodes that bracket $\Omega_{SO_2\_ini}$, θ_0, and θ, respectively. Next, the eight SO_2 Jacobian spectra are interpolated in two steps, a 2-D linear interpolation with respect to the cosines of the angles in the SZA dimension and VZA dimension followed by a 1-D linear interpolation between the two SO_2 nodes, leading to an estimated SO_2 Jacobian spectrum for SZA = θ_0, VZA = θ, RAZ = ϕ, SO_2 VCD = $\Omega_{SO_2\_ini}$, and O_3 VCD = Ω_{node1}. We repeat the above steps for the LUT with O_3 VCD = Ω_{node2} to obtain another estimated SO_2 Jacobian spectrum for the same input, but for a different O_3 profile. A final interpolation between the two O_3 nodes is then performed to generate an estimated SO_2 Jacobian spectrum for the given pixel.

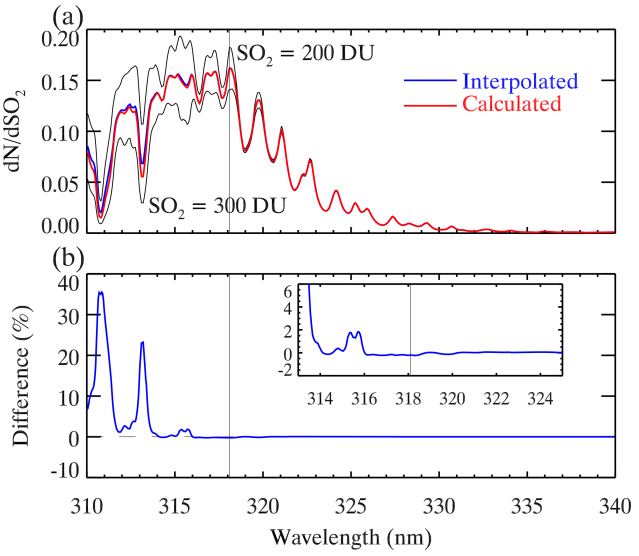

Figure 2. (a) A comparison of SO_2 Jacobians for an idealized pixel (SZA = 30°, VZA = 45°, RAZ = 90°, R = 0.05, an SO_2 plume centered at 18 km with Ω_{SO_2} = 250 DU, and a midlatitude O_3 profile with Ω_{O_3} = 375 DU) derived from direct calculation using VLIDORT (red line) and interpolation (blue line) from VLIDORT calculations for two bracketing SO_2 nodes (200 and 300 DU) shows sizable **(b)** interpolation errors at wavelengths < 315 nm, caused by nonlinearity owing to the saturation of SO_2 absorption signals. The relative difference between interpolated and directly calculated SO_2 Jacobians exceeds 30 % at wavelengths < 315 nm and remains substantial at about 2 % at ∼ 316 nm (see insert). The wavelength with the maximum interpolated SO_2 Jacobian, or the start of the fitting window for this particular example, is ∼ 318 nm and is marked with a vertical solid line in both **(a)** and **(b)**.

The SO_2 Jacobian spectrum is convolved with the OMI slit function, and then used along with the PCs from the first part of the algorithm (Fig. 1) in least squares fitting to produce an updated estimate of SO_2 VCD ($\Omega_{SO_2\_step1}$) for the pixel, which is then compared with $\Omega_{SO_2\_ini}$. If $|\Omega_{SO_2\_ini} - \Omega_{SO_2\_step1}|$ is greater than 0.1 DU or 1 % for pixels with SO_2 VCD > 100 DU, $\Omega_{SO_2\_step1}$ is used as input to the LUT to generate an updated SO_2 Jacobian spectrum. The iterations continue until the results converge or the number of iterations exceeds the upper limit (15). The same data processing steps are carried out separately for the TRL, TRM, TRU, and STL SO_2 profiles, resulting in four final estimates of SO_2 VCD for each pixel.

Table 1. Nodes of the solar zenith angle (SZA), viewing zenith angle (VZA), and SO_2 column amount, as used in the pre-computed SO_2 Jacobians lookup tables.

Parameter	Nodes														
SZA	0°		15°		30°		45°		60°		70°		77°		81°
VZA	0°		15°		30°		45°		60°		70°		75°		80°
SO_2 (DU)	0	1	5	10	50	100	200	300	400	500	600	700	800	900	1000

For volcanic SO_2 retrievals, we start with a nominal fitting window of 313–340 nm, but drop the shortest wavelengths for pixels with large SO_2 loading. As demonstrated in Fig. 2, saturation of large SO_2 absorption signals at short wavelengths leads to errors of more than 30 % in the interpolated Jacobians, even for this idealized example in which the nonlinearity in SO_2 absorption constitutes the only source of interpolation error. To reduce this error, we update the fitting window at each iteration step by locating the wavelength of the largest SO_2 Jacobian, up to 326.5 nm, and excluding all shorter wavelengths. We select 326.5 nm as the upper limit for the short end of the fitting window so that at least half of the wavelengths in the nominal window are used in the fitting. In addition, the fitting window is allowed to move to longer wavelengths only, otherwise in some cases the short end of the fitting window can change back and forth between iteration steps, resulting in non-convergence. Our approach not only helps to minimize this particular source of interpolation error but also maintains sensitivity by ensuring that those wavelengths with the largest SO_2 Jacobians are included in the spectral fitting. For an example of the shortest wavelengths used for large volcanic eruptions, refer to Fig. S3.

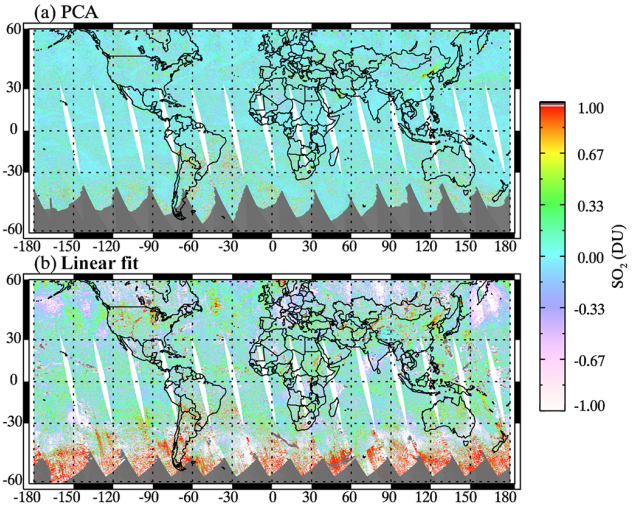

Figure 3. (a) Level 2 OMI SO_2 total vertical column density for 5 August 2006, retrieved with the OMSO2VOLCANO (PCA) algorithm assuming a lower tropospheric SO_2 plume with center of mass at 3 km altitude (TRL profile). **(b)** Same as **(a)** but for the current operational linear fit algorithm. Only pixels within the center 56 rows are plotted for both products.

3 Results: comparison with the LF algorithm

In this section, we present some examples of the volcanic SO_2 retrievals generated with the new OMSO2VOLCANO algorithm. The entire OMI data record has been reprocessed with this algorithm, and all data are publicly available (see data availability section). Here, the focus is mainly on the comparison between the OMSO2VOLCANO and the current operational LF algorithm, but we will also compare results from other algorithms wherever data are available.

3.1 Background regions

While much attention has been paid to explosive volcanic eruptions and their impacts on climate and aviation safety, the importance of degassing volcanoes is now receiving increasing recognition (see Sect. 1), despite the dearth of information on the strength of their emissions (e.g., Ge et al., 2016). OMI SO_2 retrievals can help to supply this information (e.g., Carn et al., 2013; McLinden et al., 2016; Fioletov et al., 2016), but ideally these retrievals need to have relatively low levels of noise and biases to achieve sufficient sensitivity to detect degassing sources. Here we compare the global lower tropospheric (TRL) SO_2 VCD retrieved with the operational LF and the OMSO2VOLCANO algorithms for 5 August 2006, a day with no major volcanic plumes or long-range transport of anthropogenic SO_2 in the free troposphere. As shown in Fig. 3, both products detect SO_2 signals over large emission sources such as eastern China, the Persian Gulf, and Nyiragongo volcano in eastern D.R. Congo, but the PCA-based OMSO2VOLCANO retrievals have much smaller bias and noise levels when compared with the LF retrievals. This is probably due to the fact that the PCA algorithm utilizes the full spectral content of OMI measurements, as opposed to just 10 wavelengths used in the LF algorithm. If we compare the standard deviations of the two retrievals over the SO_2-free remote Pacific, we can see that, for the majority of latitude bands from 40° S to 60° N, the standard deviations of the OMSO2VOLCANO retrievals are ∼ 0.2–0.3 DU, less than half of the standard deviation of LF retrievals (Fig. 4). The reduced biases and noise make the new OMSO2VOLCANO dataset more sensitive and stable, pro-

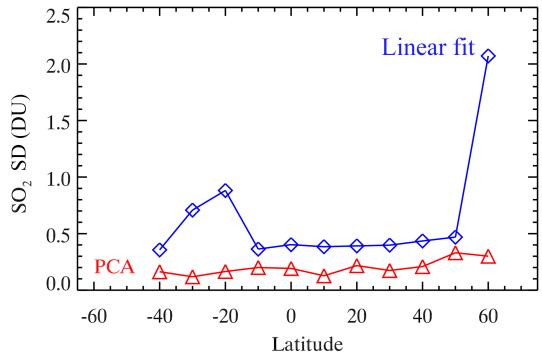

Figure 4. Standard deviation of TRL total SO_2 vertical column density retrieved for 10° latitude bands over the remote Pacific (170–180° W) on 5 August 2006 with the linear fit (blue line) and OMSO2VOLCANO (PCA, red line) algorithms.

viding enhanced long-term monitoring of continuously degassing sources. An example of this capability is provided in Sect. 4.

3.2 Kasatochi eruption in 2008

Next we examine two major volcanic eruptions during the OMI mission. The first one, the Kasatochi eruption in August 2008, is the largest to date during the OMI era (in terms of SO_2 discharge by a single explosive eruption) and has been studied extensively using several UV and infrared satellite instruments (e.g., Carn et al., 2016). Previous studies suggest that the eruption injected SO_2 to between 7 and 13 km altitude with a peak at ∼ 10 km (Kristiansen et al., 2010; Krotkov et al., 2010; Nowlan et al., 2011; Wang et al., 2013; Yang et al., 2010; Ge et al., 2016). The estimated total SO_2 mass emitted by Kasatochi varies from 1500 to 2200 kt (kiloton, 10^3 t), much greater than the ∼ 850–860 kt retrieved with the LF algorithm assuming the STL (18 km) SO_2 profile for orbits 21 635 and 21 636, the two earliest OMI overpasses after the eruption (Fig. 5). The estimated SO_2 mass for these two orbits based on LF TRM (8 km) retrievals is slightly greater, but at ∼ 950 kt it is still biased low with respect to the other estimates by almost a factor of 2, most likely due to signal saturation by high SO_2 loading in the young volcanic cloud. This apparent lack of dependence of SO_2 mass on plume height suggests that the signal saturation issue with the LF algorithm is likely more serious for TRM (and TRL) retrievals than for STL retrievals.

The OMSO2VOLCANO (PCA) retrievals (Fig. 5b and e) yield much greater estimates of SO_2 mass: ∼ 1200 kt for TRU (13 km; Fig. 5c and f) and ∼ 2000–2200 kt for TRM (8 km). The significant difference between our STL and TRU retrievals is due to the different SO_2 Jacobians between the two profiles under large SO_2 loading, as also confirmed by forward radiative transfer calculations using VLIDORT (see Fig. S5 for an example). We also note that the OMSO2VOLCANO retrieved SO_2 loadings for the two orbits agree to within 2 % for STL and TRU and to within 10 % for TRM. This suggests that the algorithm has very small cross-track biases, given that essentially the same plume was observed with different rows of the OMI instrument in these two consecutive orbits just ∼ 1.5 h apart. Taking the average of the TRU and TRM retrievals, we estimate that the OMSO2VOLCANO retrievals would have given an estimated SO_2 mass of ∼ 1700 kt for these two orbits, had a 10 km profile been used. This is ∼ 10 % larger than the offline OMI ISF retrievals (1500 kt; Yang et al., 2010) and GOME-2 optimal estimation retrievals (1600 kt; Nowlan et al., 2011), but smaller than the estimate based on the SO_2 loss rate observed over several days following the eruption (2200 kt; Krotkov et al., 2010). The total SO_2 mass for OMI orbit 21 636 estimated with a DOAS algorithm by Theys et al. (2015) is smaller at 1060 kt, but a plume height of 15 km was assumed in that study. The operational GOME-2A retrievals produced with the GDP 4.7 (GOME Data Processor) algorithm (Rix et al., 2009) for 9 August 2008 (see Fig. S4) estimate the overall SO_2 loading at 969 kt when a 15 km plume height is assumed. This falls in between the OMSO2VOLCANO STL and TRU retrievals. The SO_2 mass based on the GDP GOME-2A 6 km retrievals, in contrast, is only slightly greater at 1097 kt, much less than the optimal estimation retrievals (Nowlan et al., 2011). Like the OMI LF retrievals, this weak (and likely underestimated) dependence of SO_2 mass on plume height in the GOME-2A GDP retrievals may be due to signal saturation at shorter wavelengths.

For OMI orbit 21 650 that captured the Kasatochi plume about 24 h later, the total SO_2 mass estimated with OMSO2VOLCANO is greater than that for orbit 21 636 (∼ 1300 kt vs. ∼ 890 kt for STL, ∼ 1500 kt vs. ∼ 1200 kt for TRU, ∼ 2300 kt vs. ∼ 2000 kt for TRM). This apparent increase in the SO_2 loading over time has also been reported for other OMI retrievals for Kasatochi including the LF (1300 kt vs. 850 kt on the first day for STL retrievals), ISF (1600 kt vs. 1500 kt on the first day), and DOAS (1220 kt vs. 1060 kt on the first day) algorithms, and previously for other eruptions measured by different instruments (e.g., TOMS retrievals for the Pinatubo eruption), suggesting that the SO_2 mass may still be underestimated for highly concentrated plumes observed shortly after eruptions. This is perhaps due to the combined effects of SO_2 signal saturation and high volcanic ash and aerosol loadings. Increases in measured volcanic SO_2 loading beyond the first day of observation have also been attributed to conversion of emitted H_2S to SO_2 (e.g., Rose et al., 2000), and the new OMSO2VOLCANO retrievals promise more accurate assessments of this possibility by better eliminating the uncertainties due to SO_2 signal saturation in fresh volcanic clouds. In the Kasatochi case, a preliminary mass balance suggests that not all the observed SO_2 increase (> 100 kt) can be accounted for by conversion of detected H_2S (29 ± 10 kt of H_2S reported in the Kasatochi plume by

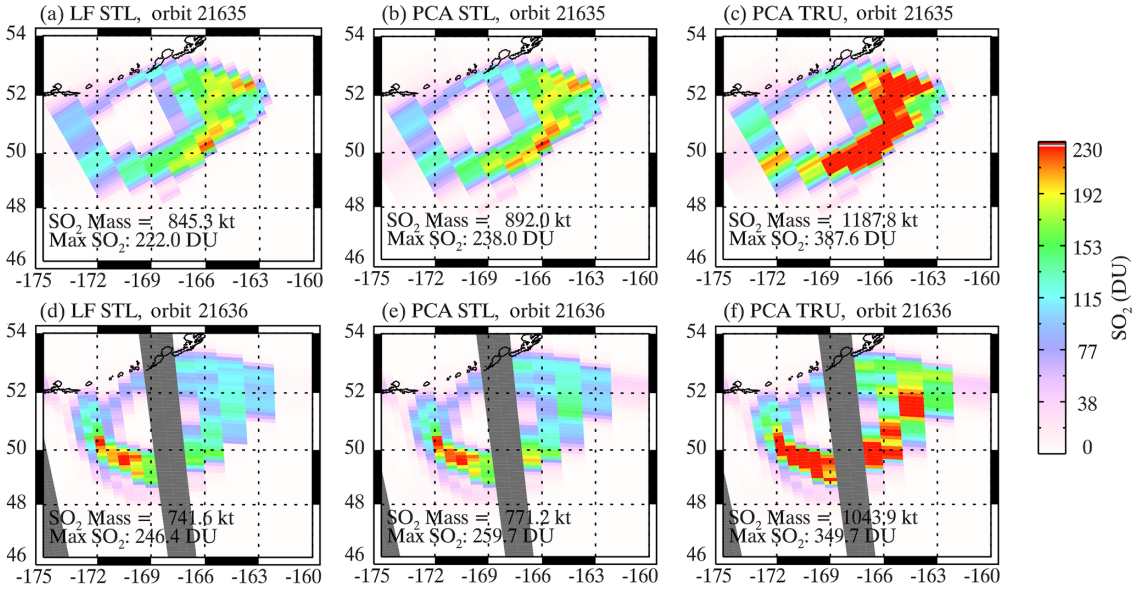

Figure 5. **(a)** OMI linear fit SO_2 retrievals assuming a lower stratospheric (STL) SO_2 profile for orbit 21 635, the first OMI overpass after the Kasatochi eruption on 8 August 2008. (**b–c**) Same as **(a)** but for OMSO2VOLCANO (PCA) retrievals assuming **(b)** the STL SO_2 profile and **(c)** an upper tropospheric (TRU) SO_2 profile. **(d)** Linear fit STL retrievals for orbit 21 636, the second OMI overpass after the eruption. (**e–f**) Same as **(d)** but for OMSO2VOLCANO **(e)** STL and **(f)** TRU retrievals. The gray-shaded rows in (**d–f**) are masked due to the OMI row anomaly. If retrievals for these masked rows are included in the calculation of the total loading, the total LF STL SO_2 mass in the domain for orbit 21 636 is 864.7 kt (see Krotkov et al., 2010), whereas PCA total mass in the domain is 897.2 kt and 1204.9 kt for STL and TRU retrievals, respectively.

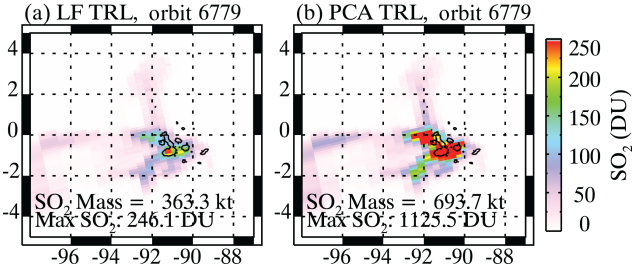

Figure 6. **(a)** OMI LF SO_2 retrievals assuming a lower tropospheric (TRL) SO_2 profile over the Galápagos Islands, from orbit 6779 on 23 October 2005, after the eruption of Sierra Negra volcano on the previous day. **(b)** Same as **(a)** but for OMSO2VOLCANO (PCA) TRL retrievals.

Clarisse et al. (2011) would yield a maximum of ∼ 74 kt of SO_2), but there are also issues with satellite sensitivity to H_2S (see Clarisse et al., 2011).

Regarding the maximum SO_2 VCDs, for orbit 21 635, the highest OMSO2VOLCANO VCDs are 238, 388, and 685 DU for STL, TRU, and TRM retrievals, respectively. In comparison, the maximum LF VCDs are smaller at 220 and 379 DU for STL and TRM, respectively. Similarly for orbit 21 636, the OMSO2VOLCANO peak VCDs are also greater at 260, 350, and 644 DU for STL, TRU, and TRM, respectively, compared with 246 and 274 DU for STL and TRM retrievals in the LF product. The DOAS algorithm developed by Theys et al. (2015) appears to produce greater peak Ω_{SO_2} for this case, with Ω_{SO_2} maxima of 382 DU for OMI orbit 21 635, and 565 DU for GOME-2 data from the same day, despite assuming a 15 km SO_2 profile and giving a smaller estimate of the overall SO_2 mass for the plume (see above). The DOAS algorithm uses the spectral window of 312–326 nm for baseline slant column SO_2 amounts (SCD1). It also retrieves additional SCDs using alternative windows (325–335 nm for SCD2 and 360–390 nm for SCD3) and determines the final fitting window based on the comparison between the SCDs. For most pixels, the baseline window is retained as the final window, but for pixels with moderate (SCD1 > 40 DU and SCD2 > SCD1) and large (SCD2 > 250 DU and SCD3 > SCD2) SO_2 signals, the longer wavelength windows of 325–335 and 360–390 nm are used, respectively (see Theys et al., 2015, for details). The SO_2 cross sections in 360–390 nm are over an order of magnitude smaller than those at the wavelengths used in PCA retrievals. Such large differences in the cross sections may contribute to the different peak SO_2 VCDs between the PCA and DOAS retrievals, but a more detailed comparison between the two algorithms will be necessary to fully understand their differences.

3.3 Sierra Negra eruption in 2005

The second example we examined was the effusive eruption of Sierra Negra (Galápagos Islands) in 2005. This eruption began on October 22 of that year and injected large amounts of SO_2 into the lower troposphere with little ash (Yang et al., 2009a), thus representing different conditions to the explosive Kasatochi eruption. The Sierra Negra volcanic plume was measured using OMI LF TRL retrievals for orbit 6779 on 23 October yielding a maximum SO_2 VCD of 246 DU and a total SO_2 mass of 363 kt (Fig. 6a). The OMSO2VOLCANO TRL retrievals (Fig. 6b) for the same orbit reveal a similar spatial distribution of the SO_2 plume but give a much greater total SO_2 mass of 694 kt, almost double that of the LF algorithm. The maximum SO_2 VCD retrieved with the OMSO2VOLCANO algorithm is extraordinarily high at $\sim$ 1125 DU, the largest detected to date by satellites. A similarly large VCD has also been retrieved for the same case with the offline OMI ISF algorithm (> 1100 DU; Yang et al., 2009a). The good agreement between the OMSO2VOLCANO and ISF algorithms suggests that both can produce less-biased retrievals than the LF algorithm but, unlike the ISF algorithm, OMSO2VOLCANO has been implemented operationally and does not require online radiative transfer calculations and instrument-specific corrections to the radiance data (i.e., soft calibration). One may notice that the difference between OMSO2VOLCANO and LF is even greater for this case than for Kasatochi, probably reflecting the more serious signal saturation issue in the LF algorithm for TRL retrievals.

4 Data continuity with the Suomi-NPP OMPS instrument

Now already in its 12th year of service, OMI is expected to continue to provide global monitoring of volcanic SO_2. However, the quality and spatial coverage of OMI measurements are presently limited by instrument issues that have developed over time. In particular, since 2009 about half of the 60 OMI rows have been rendered unusable by a partial blockage of the field of view (i.e., the OMI row anomaly; http://projects.knmi.nl/omi/research/product/rowanomaly-background.php). Several satellite instruments currently in orbit or to be launched in the near future will continue the UV satellite volcanic SO_2 data record (Carn et al., 2015, 2016). Particularly suitable for this task is the OMPS nadir mapper (OMPS-NM) on board the Suomi-NPP spacecraft (Flynn et al., 2014; Seftor et al., 2014). This platform was launched in 2011 and is flying in a sun-synchronous orbit with a local afternoon overpass time close to that of the Aura satellite (OMI). OMPS has already made several years' worth of measurements that overlap the OMI mission. This makes it possible to conduct extensive comparisons between retrievals from the two instruments in order to evaluate their consistency. Like OMI, the 2-D "push-broom" CCD detector of OMPS-NM covers the entire globe on a daily basis, allowing the total SO_2 mass to be estimated for complete volcanic clouds. However, there are challenges in the construction of a consistent volcanic SO_2 dataset between the two instruments, given the coarser spatial ($50 \times 50\,km^2$ vs. $13 \times 24\,km^2$ at nadir) and spectral (1 nm vs. $\sim$ 0.5–0.6 nm) resolution offered by OMPS-NM. For small SO_2 sources in the boundary layer, the coarser spectral resolution of OMPS may lead to $\sim$ 10 % reduction in SO_2 signals. More importantly, since an OMPS pixel is several times larger than an OMI pixel, this may lead to significant dilution of SO_2 signals for isolated small-scale plumes (see Fig. S6 for an example). As for large volcanic eruptions, multiple OMI pixels existing in a single OMPS pixel may have very different SO_2 amounts and different Jacobians, particularly for shorter wavelengths. As a result, the saturation issue discussed in Sect. 3 can have different effects on OMI and OMPS retrievals even if the two instruments are making simultaneous measurements of the same volcanic plume (see Fig. S7 for an example). Furthermore, differences in instrument calibration also need to be taken into account to minimize inter-instrument biases.

Our PCA-based retrieval approach can help to overcome these challenges, as it has small biases and requires no explicit instrument-specific corrections to the radiance data. Indeed, in a separate study (Zhang et al., 2016), we showed that the PCA PBL SO_2 algorithm was able to produce nearly unbiased retrievals for regional SO_2 pollution events between OMI and OMPS. Here, we examine the feasibility of using OMPS to continue the volcanic SO_2 emission dataset produced from OMI, for both continuously degassing volcanoes and large eruptions. The OMPS PCA volcanic SO_2 algorithm used here is almost identical to the OMSO2VOLCANO algorithm, with the exception of two implementation details: (1) we used fewer PCs in the spectral fitting (up to 15 PCs for OMPS, compared with 20 for OMI), since OMPS has approximately half the wavelengths of OMI in the same spectral fitting window; (2) we extended the OMPS retrievals to pixels with solar zenith angles up to 75° to gain more spatial coverage near the edge of the swath at high latitudes in winter months.

4.1 Long-term monitoring of SO_2 degassing from Kīlauea volcano

Kīlauea volcano is the most active of the five volcanoes on the island of Hawai'i and has been in a state of near-continuous effusive eruption since 1983. Lower tropospheric SO_2 plumes emitted from Kīlauea have been detected routinely by OMI since the start of the Aura mission (e.g., Carn et al., 2013). Here, we compare the PCA volcanic SO_2 retrievals over the Hawai'i region from both OMI and OMPS instruments (Fig. 7). To calculate the daily SO_2 mass within the domain around Kīlauea (16–21° N, 154–160° W), we first gridded OMI and OMPS TRL SO_2 retrievals to the same

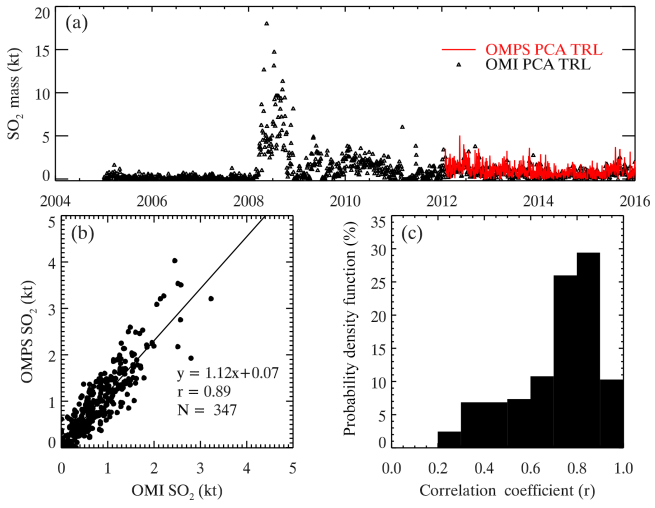

Figure 7. (a) Daily total SO_2 mass in a domain (16–21° N, 154–160° W) around the Kīlauea volcano in Hawai'i, retrieved with OMI and OMPS using the PCA algorithm assuming a lower tropospheric (TRL) SO_2 profile. Only days with at least 90 % coverage of the domain by either OMI (the first 24 rows) or OMPS (all 36 rows) are shown. **(b)** Scatter plot between OMI- and OMPS-estimated total SO_2 over the domain for days with at least 90 % spatial coverage by both OMI (the first 24 rows) and OMPS. **(c)** The probability density function of the daily spatial correlation coefficient between OMI and OMPS TRL SO_2, both gridded at 0.5° × 0.5° resolution. Only those days (∼ 200 in all) when both instruments covered over 90 % of the domain and detected over 0.5 kt of SO_2 are included.

0.5° × 0.5° horizontal resolution and then calculated the total SO_2 loading for each instrument by summing the SO_2 mass in all grid cells with SO_2 VCD > 0.4 DU. This threshold was selected to include only signals that are at least twice the retrieval noise level for the area (∼ 0.2 DU, see Fig. 4). To ensure consistency in sampling, only the first 24 rows of OMI (considered to be unaffected by the row anomaly) were used, and only those days with at least 90 % spatial coverage by these 24 rows were included in the time series plot in Fig. 7a. We applied the same SO_2 threshold and spatial coverage constraints to the OMPS data but used all 36 rows of the OMPS-NM sensor. As shown in Fig. 7a, OMI has detected substantial variability in the SO_2 loading over the area near Kīlauea, with a calm period until March 2008 and an active period during 2008–2010, followed by another relatively calm period. This is qualitatively consistent with the estimates by Carn et al. (2013) and Ge et al. (2016) using the OMI LF retrievals and also with ground observations (Elias and Sutton, 2012). OMPS provided more frequent measurements during 2012–2015 due to its more complete spatial coverage. The OMPS SO_2 time series compares well with the OMI record for the period. A regression analysis (Fig. 7b) confirms that OMPS estimates of daily regional SO_2 mass are well correlated with OMI estimates, with a correlation coefficient (r) of 0.89 and a slope of 1.12, indicating slight overestimates by OMPS as compared with OMI. Analysis using reduced major-axis regression yields a slope of 1.25, still suggesting overall consistency between OMI and OMPS. We also investigated the correlation between the spatial distributions of the OMI and OMPS PCA retrievals on a daily basis (Fig. 7c) and found that for the ∼ 200 days when both instruments detected at least 0.5 kt of SO_2 over the area, 84 % of them had r of at least 0.5 (66 % had $r > 0.7$). Only 5 of these days had $r < 0.3$ (5 February 2012, 2 October 2012, 14 May 2013, 6 November 2013, and 9 November 2014) and on all 5 days the core of the plume was covered by OMI pixels near the nadir position but by OMPS pixels near the edge of the swath. This comparison demonstrates that OMPS is capable of extending the long-term OMI record of SO_2 emissions from degassing volcanoes.

4.2 Kelut eruption in 2014

The violent explosive eruption of Mt. Kelut in Indonesia on the night of 13 February 2014 injected a volcanic plume to altitudes of ∼ 16–17 km and above (Kristiansen et al., 2015). OMSO2VOLCANO SO_2 retrievals for the OMI overpass on the following day (Fig. 8a) were able to capture the plume, but the estimated total SO_2 mass of ∼ 131 kt is certainly biased low, as a sizeable part of the plume was obscured by the OMI row anomaly. The OMPS PCA retrievals (Fig. 8b) produce a very similar spatial pattern to the OMI retrievals, and the complete plume coverage by OMPS yields a greater estimate of total SO_2 (179 kt). However, the OMPS retrievals lack some of the spatial detail offered by OMI and have a smaller maximum SO_2 VCD (47.5 DU vs. 69.3 DU); this is probably mainly due to its coarser spatial resolution (see Fig. S8 for a more detailed explanation). Given that OMI and OMPS overpasses were only 30 min apart in this case, we can combine the OMI and OMPS retrievals to produce an integrated SO_2 map that covers the plume in its entirety whilst providing fine spatial resolution where OMI data are available (Fig. 8c). This is facilitated by the very good agreement between OMI and OMPS PCA retrievals and involves assigning the SO_2 VCD from the closest OMPS pixel (based on pixel center coordinates) to each OMI row anomaly pixel. In fact, the total SO_2 mass estimated from the combined OMI+OMPS map (174 kt; Fig. 8c) agrees with the OMPS-only estimate to within 3 %. The Kelut example demonstrates that our OMPS PCA data can supplement OMI retrievals to provide complete and consistent coverage for large volcanic eruptions.

5 Conclusions

In summary, we have developed a new-generation OMI volcanic total SO_2 column amount dataset using an algorithm based on a PCA technique. The new algorithm, OMSO2VOLCANO, directly extracts spectral features (in

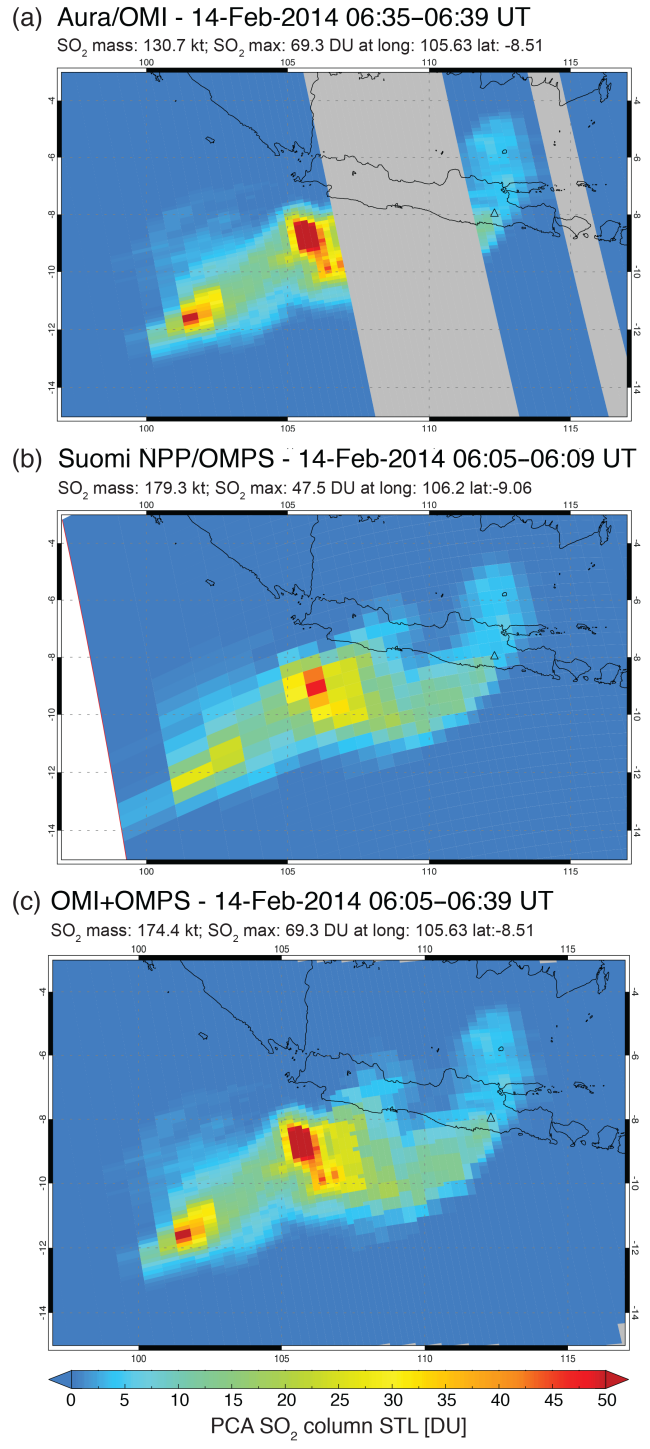

Figure 8. **(a)** The volcanic SO_2 plume from the Kelut eruption on 13 February 2014 retrieved using the OMI PCA algorithm (OMSO2VOLCANO) assuming the STL SO_2 profile on the following day. Shaded areas are masked due to the OMI row anomaly. **(b)** Same as **(a)** but for OMPS PCA retrievals. **(c)** Same as **(a)** but for the merged OMI and OMPS PCA STL SO_2 retrievals.

the form of PCs) from OMI radiances that are associated with various geophysical processes (e.g., O_3 absorption, RRS) and measurement details (e.g., wavelength shift). The algorithm then fits these PCs and SO_2 Jacobians (representing instrument sensitivity to a perturbation in column SO_2) to the measured radiances in order to estimate SO_2 while minimizing the impacts of various interferences on SO_2 retrievals. An LUT approach was developed to determine SO_2 Jacobians under various conditions such as measurement geometry (solar zenith angle, viewing zenith angle, and relative azimuth angle), SO_2 amount, O_3 amount (from OMI or OMPS total O_3 products), and the reflectivity of the underlying surface. To first order, the effects of clouds and aerosols are accounted for using a SLER derived at longer wavelengths (342.5, 354.1, 367.04 nm) and then extrapolated to our nominal fitting window of 313–340 nm. For very large volcanic plumes, SO_2 absorption may saturate at shorter wavelengths, leading to large interpolation error. To circumvent this problem, the spectral fitting window is updated dynamically at each iteration step by locating the wavelength with the maximum SO_2 Jacobian in the nominal window and dropping all shorter wavelengths. In the absence of information on SO_2 plume height, retrievals of SO_2 total column amounts are given for four different predefined SO_2 profiles with peaks at 3 (TRL), 8 (TRM), 13 (TRU), and 18 km (STL), representing typical altitudes of plumes from non-eruptive volcanic degassing, moderate eruptions, and explosive eruptions (TRU and STL), respectively. For large eruptions, OMI radiances at short wavelengths (<313 nm) may contain information on the height of the volcanic plume (e.g., Yang et al., 2009b). However, such plume height retrievals require extensive online RT calculations that are currently too computationally expensive to be implemented as part of an operational global retrieval algorithm.

Comparisons with the current operational OMI volcanic SO_2 product based on the LF algorithm and other satellite datasets suggest that the new OMSO2VOLCANO dataset has significantly lower biases and noise with respect to the LF, with the background noise reduced by half or more over the remote Pacific. For the Kasatochi eruption in 2008, the OMSO2VOLCANO retrievals give an estimated SO_2 total mass of ~ 1700 kt from OMI observations shortly after the eruption, a factor of 2 greater than LF estimates and generally in agreement with OMI ISF (Yang et al., 2010) and DOAS (Theys et al., 2015) retrievals as well as GOME-2 optimal estimation retrievals (Nowlan et al., 2011). For the Sierra Negra eruption in 2005, the OMSO2VOLCANO algorithm detects a peak SO_2 column amount of over 1100 DU. This value is consistent with that obtained using the offline ISF algorithm (Yang et al., 2009), and this concurrence suggests that, for this case, the LF algorithm underestimates peak SO_2 amounts by a large margin. Overall, the new OMSO2VOLCANO dataset has much improved data quality for both quiescent degassing volcanoes and large eruptions, when compared with the LF product. Unlike the ISF

algorithm, the OMSO2VOLCANO algorithm has been implemented operationally as it requires far less computational resources and also does not rely on instrument-specific soft calibration.

To extend the 10-year OMI volcanic SO_2 data record and to mitigate the loss of OMI spatial coverage due to the row anomaly, we have implemented the same PCA volcanic SO_2 algorithm with the Suomi-NPP OMPS instrument nadir mapper. Despite its coarser spatial and spectral resolution, the PCA retrievals with OMPS are highly consistent with those from the OMSO2VOLCANO dataset. For the area around the continuously degassing Kīlauea volcano in Hawai'i, the OMPS and OMI estimates of daily total SO_2 loading are highly correlated ($r = 0.89$, slope $= 1.12$). For large volcanic eruptions, OMPS and OMI PCA retrievals can be merged to achieve complete spatial coverage and fine measurement details, as demonstrated for the Kelut eruption in 2014. The estimated total SO_2 mass within the Kelut plume from the combined OMI–OMPS data agrees with the OMPS-only data to within 3 %, again indicating very good agreement between OMI and OMPS retrievals.

Overall, the new PCA-based OMSO2VOLCANO dataset offers enhanced sensitivity to small volcanic degassing sources and more accurate retrievals for large volcanic plumes as compared with the current operational OMI volcanic SO_2 product. The new dataset will help to improve our understanding of the impacts of volcanic emissions, and the new record will be continued with existing instruments and extended with future sensors such as the next generation of OMPS on the Joint Polar Satellite System (JPSS) spacecraft and TROPOMI (the TROPospheric Monitoring Instrument) on the Copernicus Sentinel 5 Precursor.

6 Data availability

The new-generation OMI volcanic (TRL, TRM, and STL) SO_2 product based on the OMSO2VOLCANO algorithm (OMSO2 v1.3.0) is publicly available from the NASA Goddard Earth Sciences (GES) Data and Information Services Center (DISC; http://disc.sci.gsfc.nasa.gov/Aura/data-holdings/OMI/omso2_v003.shtml). The OMI TRU SO_2 data are upon request from the corresponding author.

The Supplement related to this article is available online at doi:10.5194/amt-10-445-2017-supplement.

Competing interests. The authors declare that they have no conflict of interest.

Acknowledgements. The authors acknowledge the NASA Earth Science Division (ESD) Aura Science Team program (managed by Ken Jucks) for funding of OMI SO_2 product development and analysis. The Dutch- and Finnish-built OMI instrument is part of the NASA's Earth Observing System (EOS) Aura satellite payload. The OMI project is managed by the Royal Meteorological Institute of the Netherlands (KNMI) and the Netherlands Space Agency (NSO). Can Li acknowledges partial support from NASA's Earth Science New Investigator Program in developing the OMPS SO_2 algorithm (grant no. NNX14AI02G).

The authors would also like to thank the NASA OMPS ozone Product Evaluation and Test Element (PEATE) team for updating the OMPS calibration and producing the OMPS Level 1b and Level 2 O_3 data used in this analysis. We thank the OMI calibration team, led by KNMI, for the calibrated OMI Level 1b data used here.

Edited by: A. Richter
Reviewed by: two anonymous referees

References

Ahmad, Z., Bhartia, P. K., and Krotkov, N.: Spectral properties of backscattered UV radiation in cloudy atmospheres, J. Geophys. Res., 109, D01201, doi:10.1029/2003JD003395, 2004.

Bhartia, P. K. and Wellemeyer, C. W.: OMI TOMS-V8 Total O_3 Algorithm, Algorithm Theoretical Baseline Document: OMI Ozone Products, edited by: Bhartia, P. K., ATBD-OMI-02, version 2.0, available at: http://eospso.gsfc.nasa.gov/sites/default/files/atbd/ATBD-OMI-02.pdf (last access: 31 January 2017), 2002.

Bluth, G. J. S., Schnetzler, C. C., Krueger, A. J., and Walter, L. S.: The contribution of explosive volcanism to global atmospheric sulphur dioxide concentrations, Nature, 366, 327–329, 1993.

Burrows, J. P, Weber, M., Buchwitz, M., Rozanov, V. V., Ladstädter-Weissenmayer, A., Richter, A., de Beek, R., Hoogen, R., Bramstedt, K., Eichmann, K.-U., Eisinger, M., and Perner, D.: The Global Ozone Monitoring Experiment (GOME): Mission concept and first scientific results, J. Atmos. Sci., 56, 151–175, 1999.

Carn, S. A.: Multi-Satellite Volcanic Sulfur Dioxide (SO_2) Database Long-Term L4 Global, Version 2, Goddard Earth Science Data and Information Services Center (GES DISC), Greenbelt, MD, USA, available at: http://disc.sci.gsfc.nasa.gov/datacollection/MSVOLSO2L4_V2.html (last access: 17 June 2016), 2015.

Carn, S. A., Krueger, A. J., Arellano, S., Krotkov, N. A., and Yang, K.: Daily monitoring of Ecuadorian volcanic degassing from space, J. Volcanol. Geoth. Res., 176, 141–150, 2008.

Carn, S. A., Krueger, A. J., Krotkov, N. A., Yang, K., and Evans, K.: Tracking volcanic sulfur dioxide clouds for aviation hazard mitigation, Nat. Hazards, 51, 325–343, doi:10.1007/s11069-008-9228-4, 2009.

Carn, S. A., Krotkov, N. A., Yang, K., and Krueger, A. J.: Measuring global volcanic degassing with the Ozone Monitoring Instrument (OMI), in: Remote Sensing of Volcanoes and Volcanic Processes: Integrating Observation and Modeling, edited by: Pyle, D. M., Mather, T. A., and Biggs, J., Geol. Soc. Lon, Special Publications, 380, doi:10.1144/SP380.12, 2013.

Carn, S. A., Clarisse, L., and Prata, A. J.: Multi-decadal satellite measurements of global volcanic degassing, J. Volcanol. Geoth. Res., 311, 99–134, doi:10.1016/j.jvolgeores.2016.01.002, 2016.

Clarisse, L., Coheur, P.-F., Chefdeville, S., Lacour, J.-L., Hurtmans, D., and Clerbaux, C.: Infrared sat- ellite observations of hydrogen sulfide in the volcanic plume of the August 2008 Kasatochi eruption, Geophys. Res. Lett., 38, L10804, doi:10.1029/2011GL047402, 2011.

Dave, J. V.: Meaning of successive iteration of the auxiliary equation of radiative transfer, Astrophys. J., 140, 1292–1303, 1964.

Eisinger, M. and Burrows, J. P.: Tropospheric Sulfur Dioxide observed by the ERS-2 GOME Instrument, Geophys. Res. Lett., 25, 4177–4180, 1998.

Elias, T. and Sutton, A. J.: Sulfur dioxide emission rates from Kīlauea Volcano, Hawai'i, 2007–2010, US Geological Survey Open File Report, 2012–1107, available at: http://pubs.usgs.gov/of/2012/1107/of2012-1107_text.pdf (last access: 31 January 2017), 2012.

Fioletov, V. E., McLinden, C. A., Krotkov, N., and Li, C.: Lifetimes and emissions of SO_2 from point sources estimated from OMI, Geophys. Res. Lett., 42, 1969–1976, doi:10.1002/2015GL063148, 2015.

Fioletov, V. E., McLinden, C. A., Krotkov, N., Li, C., Joiner, J., Theys, N., Carn, S., and Moran, M. D.: A global catalogue of large SO_2 sources and emissions derived from the Ozone Monitoring Instrument, Atmos. Chem. Phys., 16, 11497–11519, doi:10.5194/acp-16-11497-2016, 2016.

Flynn, L., Long, C., Wu, X., Evans, R., Beck, C. T., Petropavlovskikh, I., McConville, G., Yu, W., Zhang, Z., Niu, J., Beach, E., Hao, Y., Pan, C., Sen, B., Novicki, M., Zhou, S., and Seftor, C.: Performance of the Ozone Mapping and Profiler Suite (OMPS) products, J. Geophys. Res.-Atmos., 119, 6181–6195, doi:10.1002/2013JD020467, 2014.

Ge, C., Wang, J., Carn, S., Yang, K., Ginoux, P., and Krotkov, N.: Satellite-based global volcanic SO_2 emissions and sulfate direct radiative forcing during 2005–2012, J. Geophys. Res.-Atmos., 121, 3446–3464, doi:10.1002/2015JD023134, 2016.

He, H., Vinnikov, K. Y., Li, C., Krotkov, N. A., Jongeward, A. R., Li, Z., Stehr, J. W., Hains, J. C., and Dickerson, R. R.: Response of SO_2 and particulate air pollution to local and regional emission controls: A case study in Maryland, Earth's Future, 4, 94–109, doi:10.1002/2015EF000330, 2016.

Hsu, N. C., Li, C., Krotkov, N. A., Liang, Q., Yang, K., and Tsay, S. C.: Rapid transpacific transport in autumn observed by the A-train satellites, J. Geophys. Res.-Atmos., 117, D06312, doi:10.1029/2011JD016626, 2012.

Kristiansen, N. I., Stohl, A., Prata, A. J., Richter, A., Eckhardt, S., Seibert, P., Hoffmann, A., Ritter, C., Bitar, L., Duck, T. J., and Stebel, K.: Remote sensing and inverse transport modeling of the Kasatochi eruption sulfur dioxide cloud, J. Geophys. Res., 115, D00L16, doi:10.1029/2009JD013286, 2010.

Kristiansen, N. I., Prata, A. J., Stohl, A., and Carn, S. A.: Stratospheric volcanic ash emissions from the 13 February 2014 Kelut eruption, Geophys. Res. Lett., 42, 588–596, doi:10.1002/2014GL062307, 2015.

Krotkov, N. A., Carn, S. A., Krueger, A. J., Bhartia, P. K., and Yang, K.: Band residual difference algorithm for retrieval of SO_2 from the aura Ozone Monitoring Instrument (OMI), IEEE T. Geosci. Remote, 44, 1259–1266, 2006.

Krotkov, N. A., McClure, B., Dickerson, R. R., Carn, S. A., Li, C., Bhartia, P. K., Yang, K., Krueger, A. J., Li, Z. Q., Levelt, P. F., Chen, H. B., Wang, P. C., and Lu, D. R.: Validation of SO_2 retrievals from the Ozone Monitoring Instrument over NE China, J. Geophys. Res., 113, D16S40, doi:10.1029/2007jd008818, 2008.

Krotkov, N., Schoeberl, M., Morris, G., Carn, S., and Yang, K.: Dispersion and lifetime of the SO_2 cloud from the August 2008 Kasatochi eruption, J. Geophys. Res., 115, D00L20, doi:10.1029/2010JD013984, 2010.

Krotkov, N. A., McLinden, C. A., Li, C., Lamsal, L. N., Celarier, E. A., Marchenko, S. V., Swartz, W. H., Bucsela, E. J., Joiner, J., Duncan, B. N., Boersma, K. F., Veefkind, J. P., Levelt, P. F., Fioletov, V. E., Dickerson, R. R., He, H., Lu, Z., and Streets, D. G.: Aura OMI observations of regional SO_2 and NO_2 pollution changes from 2005 to 2015, Atmos. Chem. Phys., 16, 4605–4629, doi:10.5194/acp-16-4605-2016, 2016.

Krueger, A. J.: Sighting of El Chichón sulfur dioxide clouds with the Nimbus 7 Total Ozone Mapping Spectrometer, Science, 220, 1377–1378, 1983.

Krueger, A. J., Walter, L. S., Bhartia, P. K., Schnetzler, C. C., Krotkov, N. A., Sprod, I., and Bluth, G. J. S.: Volcanic sulphur dioxide measurements from the total ozone mapping spectrometer instruments, J. Geophys. Res., 100, 14057–14076, 1995.

Lee, C., Richter, A., Weber, M., and Burrows, J. P.: SO_2 Retrieval from SCIAMACHY using the Weighting Function DOAS (WF-DOAS) technique: comparison with Standard DOAS retrieval, Atmos. Chem. Phys., 8, 6137–6145, doi:10.5194/acp-8-6137-2008, 2008.

Levelt, P. F., van den Oord, G. H. J., Dobber, M. R., Malkki, A., Visser, H., de Vries, J., Stammes, P., Lundell, J. O. V., and Saari, H.: The Ozone Monitoring Instrument, IEEE T. Geosci. Remote, 44, 1093–1101, 2006.

Li, C., Krotkov, N. A., Dickerson, R. R., Li, Z., Yang, K., and Chin, M.: Transport and evolution of a pollution plume from northern China: A satellite-based case study, J. Geophys. Res., 115, D00K03, doi:10.1029/2009JD012245, 2010a.

Li, C., Zhang, Q., Krotkov, N. A., Streets, D. G., He, K., Tsay, S.-C., and Gleason, J. F.: Recent large reduction in sulfur dioxide emissions from Chinese power plants observed by the Ozone Monitoring Instrument, Geophys. Res. Lett., 37, L08807, doi:10.1029/2010GL042594, 2010b.

Li, C., Joiner, J., Krotkov, N. A., and Bhartia, P. K.: A fast and sensitive new satellite SO_2 retrieval algorithm based on principal component analysis: Application to the ozone monitoring instrument, Geophys. Res. Lett., 40, 6314–6318, doi:10.1002/2013GL058134, 2013.

Li, C., Joiner, J., Krotkov, N. A., and Dunlap, L.: A new method for global retrievals of HCHO total columns from the Suomi National Polar-orbiting Partnership Ozone Mapping and Profiler Suite. Geophys. Res. Lett., 42, 2515–2522, doi:10.1002/2015GL063204, 2015.

Lu, Z., Streets, D. G., Zhang, Q., Wang, S., Carmichael, G. R., Cheng, Y. F., Wei, C., Chin, M., Diehl, T., and Tan, Q.: Sulfur dioxide emissions in China and sulfur trends in East Asia since 2000, Atmos. Chem. Phys., 10, 6311–6331, doi:10.5194/acp-10-6311-2010, 2010.

McCormick, M. P., Thomason, L. W., and Trepte, C. R.: Atmospheric effects of Mt. Pinatubo eruption, Nature, 373, 399–404, 1995.

McLinden, C. Fioletov, V., Shephard, M., Krotkov, N., Li, C., Martin, R. V., Moran, M. D., and Joiner, J.: Space-based detection of missing SO_2 sources of global air pollution, Nat. Geosci., 9, 496–500, doi:10.1038/NGEO2724, 2016.

McPeters, R. D.: The atmospheric SO_2 budget for Pinatubo derived from NOAA-11 SBUV/2 spectral data, Geophys. Res. Lett., 20, 1971–1974, 1993.

Nowlan, C. R., Liu, X., Chance, K., Cai, Z., Kurosu, T. P., Lee, C., and Martin, R. V.: Retrievals of sulfur dioxide from the Global Ozone Monitoring Experiment 2 (GOME-2) using an optimal estimation approach: Algorithm and initial validation, J. Geophys. Res., 116, D18301, doi:10.1029/2011JD015808, 2011.

Ridley, D. A., Solomon, S., Barnes, J. E., Burlakov, V. D., Deshler, T., Dolgii, S. I., Herber, A. B., Nagai, T., Neely, R. R., Nevzorov, A. V., Ritter, C., Sakai, T., Santer, B. D., Sato, M., Schmidt, A., Uchino, O., and Vernier, J. P.: Total volcanic stratospheric aerosol optical depths and implications for global climate change, Geophys. Res. Lett., 41, 7763–7769, doi:10.1002/2014GL061541, 2014.

Rix, M., Valks, P., Hao, N., van Geffen, J., Clerbaux, C., Clarisse, L., Coheur, P.-F., Loyola, D. G., Erbertseder, T., Zimmer, W., and Emmadi, S.: Satellite monitoring of volcanic sulfur dioxide emissions for early warning of volcanic hazards, IEEE J. Selec. Top. Appl. Earth Obs. Remote Sens., 2, 196–206, 2009.

Robock, A. and Mao, J.: The volcanic signal in surface temperature observations, J. Climate, 8, 1086–1103, 1995.

Robock, A., Adams, T., Moore, M., Oman, L., and Stenchikov, G.: Southern hemisphere atmospheric circulation effects of the 1991 Mount Pinatubo eruption, Geophys. Res. Lett., 34, L23710, doi:10.1029/2007GL031403, 2007.

Rose, W. I., Bluth, G. J. S., and Ernst, G. G. J.: Integrating retrievals of volcanic cloud characteristics from satellite remote sensors – a summary, Philos. T. R. Soc. A, 358, 1585–1606, 2000.

Santer, B. D., Bonfils, C., Painter, J. F., Zelinka, M. D., Mears, C., Solomon, S., Schmidt, G. A., Fyfe, J. C., Cole, J. N. S., Nazarenko, L., Taylor, K. E., and Wentz, F. J.: Volcanic contribution to decadal changes in tropospheric temperature, Nat. Geosci., 7, 185–189, doi:10.1038/ngeo2098, 2014.

Schmidt, A., Carslaw, K. S., Mann, G. W., Rap, A., Pringle, K. J., Spracklen, D. V., Wilson, M., and Forster, P. M.: Importance of tropospheric volcanic aerosol for indirect radiative forcing of climate, Atmos. Chem. Phys., 12, 7321–7339, doi:10.5194/acp-12-7321-2012, 2012.

Seftor, C. J., Jaross, G., Kowitt, M., Haken, M., Li, J., and Flynn, L. E.: Postlaunch performance of the Suomi National Polar-orbiting Partnership Ozone Mapping and Profiler Suite (OMPS) nadir sensors, J. Geophys. Res.-Atmos., 119, 4413–4428, doi:10.1002/2013JD020472, 2014.

Solomon, S., Daniel, J. S., Neely, R. R., Vernier, J.-P., Dutton, E. G., and Thomason, L. W.: The persistently variable "background" stratospheric aerosol layer and global climate change, Science, 333, 866–870, doi:10.1126/science.1206027, 2011.

Spurr, R.: LIDORT and VLIDORT: Linearized Pseudo-Spherical Scalar and Vector Discrete Ordinate Radiative Transfer Models for use in Remote Sensing Retrieval Problems, Light Scattering Reviews, edited by: Kokhanovsky, A., Springer, Berlin, Heidelberg, 3, doi:10.1007/978-3-540-48546-9, 2008.

Stenchikov, G., Robock, A., Ramaswamy, V., Schwarzkopf, M. D., Hamilton, K., and Ramachandran, S.: Arctic Oscillation response to the 1991 Mount Pinatubo eruption: Effects of volcanic aerosols and ozone depletion, J. Geophys. Res., 107, 4803, doi:10.1029/2002JD002090, 2002.

Stohl, A., Prata, A. J., Eckhardt, S., Clarisse, L., Durant, A., Henne, S., Kristiansen, N. I., Minikin, A., Schumann, U., Seibert, P., Stebel, K., Thomas, H. E., Thorsteinsson, T., Tørseth, K., and Weinzierl, B.: Determination of time- and height-resolved volcanic ash emissions and their use for quantitative ash dispersion modeling: the 2010 Eyjafjallajökull eruption, Atmos. Chem. Phys., 11, 4333–4351, doi:10.5194/acp-11-4333-2011, 2011.

Theys, N., De Smedt, I., van Gent, J., Danckaert, T., Wang, T., Hendrick, F., Stavrakou, T., Bauduin, S., Clarisse, L., Li, C., Krotkov, N., Yu, H., Brenot, H., and Van Roozendael, M.: Sulfur dioxide vertical column DOAS retrievals from the Ozone Monitoring Instrument: Global observations and comparison to ground-based and satellite data, J. Geophys. Res.-Atmos., 120, 2470–2491, doi:10.1002/2014jd022657, 2015.

Vernier, J.-P., Thomason, L. W., Pommereau, J. P., Bourassa, A., Pelon, J., Garnier, A., Hauchecorne, A., Blanot, L., Trepte, C., Degenstein, D., and Vargas, F.: Major influence of tropical volcanic eruptions on the stratospheric aerosol layer during the last decade, Geophys. Res. Lett., 38, L12807, doi:10.1029/2011GL047563, 2011.

Wang, J., Park, S., Zeng, J., Ge, C., Yang, K., Carn, S., Krotkov, N., and Omar, A. H.: Modeling of 2008 Kasatochi volcanic sulfate direct radiative forcing: assimilation of OMI SO_2 plume height data and comparison with MODIS and CALIOP observations, Atmos. Chem. Phys., 13, 1895–1912, doi:10.5194/acp-13-1895-2013, 2013.

Yang, K., Krotkov, N., Krueger, A., Carn, S., Bhartia, P., and Levelt, P.: Retrieval of large volcanic SO_2 columns from the Aura Ozone Monitoring Instrument: Comparison and limitations, J. Geophys. Res., 112, D24S43, doi:10.1029/2007JD008825, 2007.

Yang, K., Krotkov, N. A., Krueger, A. J., Carn, S. A., Bhartia, P. K., and Levelt, P. F.: Improving retrieval of volcanic sulfur dioxide from backscattered UV satellite observations, Geophys. Res. Lett., 36, L03102, doi:10.1029/2008GL036036, 2009a.

Yang, K., Liu, X., Krotkov, N. A., Krueger, A. J., and Carn, S. A.: Estimating the altitude of volcanic sulfur dioxide plumes from space borne hyperspectral UV measurements, Geophys. Res. Lett., 36, L10803, doi:10.1029/2009GL038025, 2009b.

Yang, K., Liu, X., Bhartia, P. K., Krotkov, N., Carn, S., Hughes, E., Krueger, A., Spurr, R., and Trahan, S.: Direct retrieval of sulfur dioxide amount and altitude from spaceborne hyperspectral UV measurements: Theory and application, J. Geophys. Res., 115, D00L09, doi:10.1029/2010JD013982, 2010.

Yuan, T., Remer, L. A., and Yu, H.: Microphysical, macrophysical and radiative signatures of volcanic aerosols in trade wind cumulus observed by the A-Train, Atmos. Chem. Phys., 11, 7119–7132, doi:10.5194/acp-11-7119-2011, 2011.

Zhang, Y., Li, C., Krotkov, N. A., and Joiner, J.: Continuation of long-term global SO_2 pollution monitoring from OMI to OMPS, Atmos. Meas. Tech. Discuss., doi:10.5194/amt-2016-226, in review, 2016.